crystals

MDPI

Communication

Building Manganese Halide Hybrid Materials with 0D, 1D, and 2D Dimensionalities

Anna Peoble, Kandee Gallegos, Michael O. Ozide and Raúl Castañeda *

Department of Chemistry, New Mexico Highlands University, Las Vegas, NM 87701, USA; apeoble@live.nmhu.edu (A.P.); kgallegos7@live.nmhu.edu (K.G.); mozide@live.nmhu.edu (M.O.O.)
* Correspondence: lrcastaneda@nmhu.edu

Abstract: In recent years, metal-halide hybrid materials have attracted considerable attention because materials, such as lead-iodide perovskites, can have excellent properties as photovoltaics, light-emitting devices, and photodetectors. These materials can be obtained in different dimensionalities (1D, 2D, and 3D), which directly affects their properties. In this article, we built 0D, 1D, and 2D manganese halide materials with 3-aminopyridine (3AP) or 4-ethylpyridine (4EtP). Two isomorphic complexes with 3AP and manganese chloride (**[$MnCl_2$(3AP)$_4$]**) or manganese bromide (**[$MnBr_2$(3AP)$_4$]**) were obtained with the amino group in 3AP assisting in the formation of 0D structures via hydrogen bonding. By modifying the reaction conditions, 3AP can also be used to build a 2D coordination polymer with manganese chloride (**[$MnCl_3$3AP]$^-$ [3APH]$^+$**). Unlike 3AP, 4EtP does not provide the opportunity for hydrogen bonding, leading to the formation of two additional isomorphic compounds built of individual 1D chains with manganese chloride (**{$MnCl_3$(4EtP)$_2$}$_n$**) and manganese bromide (**{$MnBr_2$(4EtP)$_2$}$_n$**). In the visible region, the 0D and 1D manganese halide compounds have similar photoluminescence properties; however, 0D and 1D have different near-IR emissions. In conclusion, hydrogen-bonding groups can play a role in the formation of discrete manganese-halide units, 1D halide chains, or 2D polymeric sheets.

Keywords: perovskite dimensionality; luminescent materials; manganese-halide hybrid materials; isomorphic structures

check for updates

Citation: Peoble, A.; Gallegos, K.; Ozide, M.O.; Castañeda, R. Building Manganese Halide Hybrid Materials with 0D, 1D, and 2D Dimensionalities. *Crystals* **2023**, *13*, 1634. https://doi.org/10.3390/cryst13121634

Academic Editors: Simona Nica and Pedro Netto Batalha

Received: 20 October 2023
Revised: 12 November 2023
Accepted: 21 November 2023
Published: 25 November 2023

Copyright: © 2023 by the authors. Licensee MDPI, Basel, Switzerland. This article is an open access article distributed under the terms and conditions of the Creative Commons Attribution (CC BY) license (https://creativecommons.org/licenses/by/4.0/).

1. Introduction

Hybrid metal-halide perovskites (MHPs) have recently attracted attention due to their interesting properties that make them candidates for different applications, including, but not limited to, photovoltaics [1–4], transistors [5,6], light-emitting diodes (LEDs) [7,8], and memory devices [9,10]. These materials mostly contain three main components: a divalent cation, which is frequently lead, a nitrogen-based cation, and halide anions. Since lead is a toxic element, research has been conducted to replace this element with different options [11,12]. In this paper, we use manganese halide compounds to build materials emitting in the near-infrared (NIR) region. Unlike Pb^{2+} and other M^{2+} cations, manganese can be tetracoordinated, pentacoordinated, hexacoordinated, or even, in a few examples, produce higher coordination numbers [13–15]. Therefore, predicting the desired product of manganese halides is more challenging than other metal ions. While extensive studies have been performed on tetrahedral 0D manganese halides, in part due to their excellent emission properties [16,17], less studies have been performed on octahedral 1D or 2D materials. Additionally, the dimensionality of manganese halide materials affects the type of emission they produce [16]. For example, molecular 0D tetrahedral complexes emit a yellow or green color, and as the material increases the number of manganese ions coordinated within the same framework [18], a red shift is observed, leading to an NIR emission in 1D materials [19]. In this article, we present the synthesis of hybrid manganese-halide materials comprised of ligands 3-aminopyridine (3AP) or 4-ethyl-pyridine (4EtP)

and chloride or bromide. Our results show that a change in the substituents on a pyridine ligand can lead to materials with different dimensionalities. Changing the dimensionality of a manganese halide can be achieved in a variety of ways. First, this can be performed by changing the coordination sphere of manganese, in addition to varying the reaction conditions (pH or solvent) and the ratios of the components [20]. Second, it is also possible to modify or add different functional groups to the organic moiety. Finally, a variation in the synthetic routes used in this work is the coordination of a nitrogen base to a manganese ion. For example, 3-aminopyridine (3AP) can lead to 0D complexes or 2D coordination polymers when used as ligand/or cation, respectively.

2. Results and Discussion

While attempting to construct 1D coordination polymers with 3AP and manganese(II) chloride or manganese(II) bromide, two isomorphic complexes with the triclinic $P\bar{1}$ space group (Table 1) were obtained. These complexes had the formula **[$MnX_2(3AP)_4$]**, and to simplify the description, only **[$MnCl_2(3AP)_4$]** was discussed with the respective distances for the bromine analog. In the asymmetric unit, the manganese ion is located in an inversion center and, as a result, the asymmetric unit contains only one halide atom and two 3AP ligands. Both complexes have the same trans-octahedral coordination, with four 3AP ligands coordinated in the equatorial position and two halide atoms coordinated in the axial position (Figure 1a). An overlay of **[$MnX_2(3AP)_4$]** showed minimal differences with the rms of 0.0746 (Figure 1b). The coordination is best described as an elongated octahedron because the Mn-Cl and Mn-Br distances (2.561(2) Å and 2.7304(3) Å, respectively) are longer than the average Mn-N distances in both complexes (2.31 Å). It should be noted that three other structures similar to **[$MnX_2(3AP)_4$]** were found in the CSD database with $MnCl_2$ and pyridine [21], $MnCl_2$ and nicotinic acid [22], and $MnBr_2$ and 3-cyanopyridine [23]. Additionally, two isomorphs with cadmium [24] (**[$CdCl_2(3AP)_4$]**) and cobalt [25] (**[$CoCl_2(3AP)_4$]**) were found in the CSD database. Only the pyridine nitrogen atom was coordinated to the manganese ion, while the amino atom assisted crystal packing by hydrogen bonding (Figure 2). The three weak hydrogen bonds observed in both isomorphic structures were longer than the sum of the van der Waals radii of nitrogen and the halide (N-3A...X1, N-3B...X1, and N-4A...X1; Table 2). These weak hydrogen bonds are the same as those observed in **[$CdCl_2(3AP)_4$]** and **[$CoCl_2(3AP)_4$]**, which exemplify the importance of weak interactions in the crystal lattice. Potentially, another isomorphic structure of **[$MX_2(3AP)_4$]** can be obtained with Fe^{2+}. One tool that can be used to compare hydrogen bonds from N-H groups is infrared spectroscopy (IR) [26]. Our results show near-identical IR spectra for **[$MnX_2(3AP)_4$]** (Figure S1), with the main difference being a shift of symmetric N-H stretching at 3372 cm^{-1} in the chloride complex as compared to 3384 cm^{-1} in bromide. In summary, IR indicates the same molecular framework in both structures with slightly different hydrogen bonding results due to the molecular difference between chlorine and bromine.

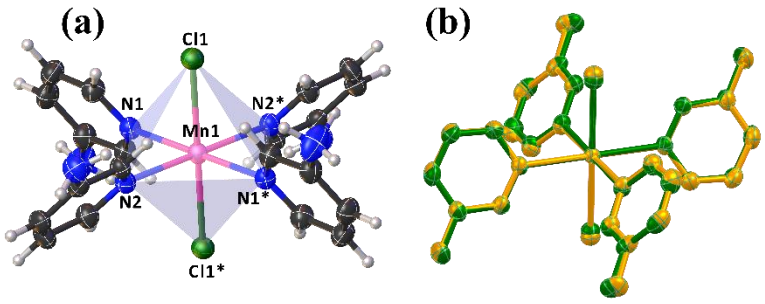


Figure 1. (**a**) View of the individual molecule of **[$MnCl_2(3AP)_4$]** and (**b**) overlays of **[$MnCl_2(3AP)_4$]** (green) and **[$MnBr_2(3AP)_4$]** (orange). Thermal ellipsoids are drawn with a 50% probability, and symmetry-related positions are indicated with the symbol *.

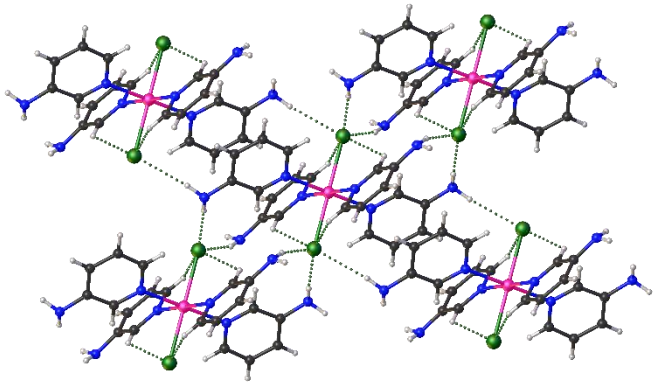


Figure 2. Crystal packing view of **[$MnCl_2$(3AP)$_4$]** along *c* axis.

Table 1. Selected crystallographic data.

Abbreviation	[$MnCl_2$(3AP)$_4$]	[$MnBr_2$(3AP)$_4$]	[$MnCl_3$3AP]$^-$ [3APH]$^+$	{$MnCl_2$(4EtP)$_2$}$_n$	{MnBr2(4EtP)2}$_n$
Empirical formula	$C_{20}H_{24}Cl_2MnN_8$	$C_{20}H_{24}Br_2MnN_8$	$C_{44}H_{44}Cl_{12}Cu_2Mn_4N_{28}O_2$	$C_{14}H_{18}Cl_2MnN_2$	$C_{14}H_{18}Br_2MnN_2$
Formula weight	502.31	591.23	350.53	340.14	429.06
Temperature (K)	100	100	100	100	100
Crystal system	Triclinic	Triclinic	Monoclinic	Monoclinic	Monoclinic
Space group	*P*$\bar{1}$	*P*$\bar{1}$	$P2_1/c$	*C*2/c	*C*2/c
a (Å)	7.974(5)	8.154(1)	11.749(3)	24.06(3)	23.671(2)
b (Å)	8.823(6)	8.856(1)	10.478(3)	3.875(5)	3.9513(4)
c (Å)	10.072(6)	10.134(1)	14.676(4)	17.91(2)	18.167(2)
α (°)	97.60(2)	98.018(4)	90	90	90
β (°)	91.84(2)	91.186(3)	107.711(7)	114.11(4)	112.722(2)
γ (°)	113.93(2)	114.446(3)	90	90	90
Volume (Å^3)	639.0(7)	657.2(2)	1721.1(8)	1524(3)	1567.3(3)
Z	1	1	4	4	4
ρ_{calc} (g/mL)	1.305	1.494	1.353	1.483	1.818
μ (mm^{-1})	0.748	3.564	1.221	1.204	5.929
F(000)	259	295	708	700	844
Data collection range (°)	4.1 to 53.9	4 to 58	3.6 to 53.5	3.7 to 50.6	3.7 to 51.3
Reflections collected	7961	16035	19781	7526	1483
Independent reflections	2773	3446	3648	1378	1483
Goof on F^2	1.086	1.041	1.067	1.050	1.085
R_1 [$I \geq 2\sigma$ (I)]	0.0243	0.0212	0.0269	0.0292	0.0296
wR_2 all reflections	0.0685	0.0539	0.0717	0.0578	0.0685
H-atom treatment	Mixed	Mixed	Mixed	Constrained	Constrained

Table 2. Hydrogen bond details of **[$MnCl_2$(3AP)$_4$]** and **[$MnBr_2$(3AP)$_4$]**.

D-H···A	D-H Distance (Å)	H···A Distance (Å)	D-A Distance (Å)	D-H···A Angle (°)
[Mn^{II}(3AP)$_4Cl_2$]				
N3-H3A···Cl1	0.892(13)	2.639(14)	3.523(3)	171.5(15)
N3-H3B···Cl1	0.878(14)	2.522(14)	3.397(2)	175.0(16)
N4-H4A···Cl1	0.887(15)	2.549(16)	3.414(2)	165(2)
[Mn^{II}(3AP)$_4Br_2$]				
N3-H3A···Br1	0.845(15)	2.803(17)	3.616(2)	162(2)
N3-H3B···Br1	0.849(15)	2.661(16)	3.507(2)	175(2)
N4-H4A···Br1	0.857(16)	2.672(18)	3.509(2)	166(2)

Using 3AP with the addition of an equimolar amount of hydrochloric acid during the reaction allows the synthesis of a layered 2D structure with the formula **[$MnCl_3$3AP]$^-$[3APH]$^+$** (Figure 3a). This structure has two independent layers (Figure 3b). The first layer is a 2D coordination polymer with the asymmetric unit containing one manganese(II) ion, one 3AP ligand, and three chlorine ions (**[$MnCl_3$3AP]$^-$**). The second layer has $3APH^+$ acting only as a cation to balance the overall charge. The coordination sphere around the manganese(II) ion has four chlorine and two nitrogen atoms. The first nitrogen atom comes from the

pyridine ring in 3AP (N1), and the second one from an amino group (N2) in a different 3AP molecule (Figure 2a). One of the chlorine ions (Cl2) is duplicated by an inversion center and acts as a bridge to a second manganese ion (Figure 2a). Unlike the 0D unit, 3AP bridges different manganese ions resulting in a 2D coordination polymer. In summary, the 2D layer is constructed by a manganese trichloride dimer that is bridged by 3AP ligands, as it can be seen on top of this layer (Figure S4). A similar coordination sphere was previously discovered with 2-aminopyridine [27], although this compound crystallized in 1D chains. To the best of our knowledge, **[MnCl$_3$3AP]$^-$[3APH]$^+$** represents the first 2D coordination polymer reported with manganese(II) chloride and a nitrogen-based ligand. Finally, the synthesis of the bromine analog **[MnBr$_3$3AP]$^-$[3APH]$^+$** was not possible in a number of different reaction conditions.

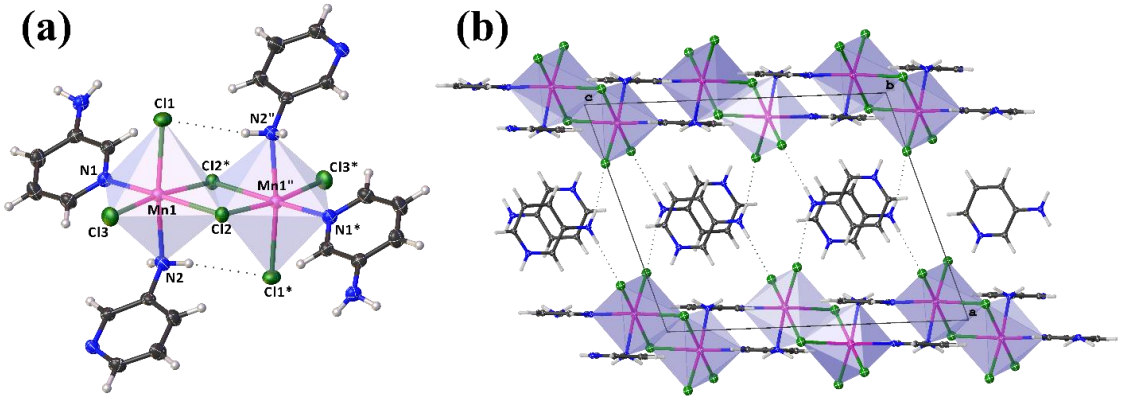


Figure 3. (**a**) Dimer unit of **[MnCl$_3$3AP]$^-$[3APH]$^+$** and (**b**) view of distinct layers along the *c* axis in **[MnCl$_3$3AP]$^-$[3APH]$^+$**. Blue octahedrons highlight the manganese core. Symmetry-related positions are indicated with the symbol *.

Surprisingly, using 4-ethylpyridine (4EtP) in the same reaction conditions as 3AP led to the formation of 1D chain structures with the formulas **{MnCl$_2$(4EtP)$_2$}$_n$** and **{MnBr$_2$(4EtP)$_2$}$_n$** (Figure 4). These 1D chain structures were isomorphic with the *C*2/*c* space group (Table 1). To simplify the description, only **{MnCl$_2$-(4EtP)$_2$}$_n$** was discussed with the respective distances for the bromine analog. A trans-octahedral coordination around the manganese ion was observed, with two 4EtP ligands coordinated in axial positions, and four halide atoms coordinated in the equatorial plane, each of them bridging a separate manganese ion in an edge-sharing fashion (Figure 4). The coordination polyhedron is best described as a elongated octahedron as the Mn-N distance is shorter than the Mn-X distance. In the asymmetric unit, the manganese ion is located in a C_2 axis that reproduces 4EtP by symmetry. On the other hand, the halide is located near an inversion center, and it is reproduced by the C_2 axis and inversion center. As a result, the asymmetric unit contains three components: one 4EtP ligand, one manganese center, and one halide. Despite the highly symmetrical nature of these 1D chain structures, only three other structures with similar 1D chains were found in the literature: benzotriazole [28], benzo-2,1,3-selenenadiazole [29], and 3-cyanopyridine [23]. As expected, similar IR and Raman spectra were observed in these 1D chains (Figures S2 and S3), indicating the same framework.

In the solid state, the 0D and 1D materials studied had very similar broad photoluminescence (PL) values from 400 to 550 nm (Figure 5a), with the maximum emission at 468 nm, and near-identical peak patterns. Unexpectedly, the 2D material **[MnCl$_3$3AP]$^-$[3APH]$^+$** lacked any relevant PL when compared to the rest of the materials. The main differences between the 0D and 1D materials were observed in the NIR region. There was an additional emission band at 760 nm observed in the 1D chains that was absent from the 0D units (Figure 5b).

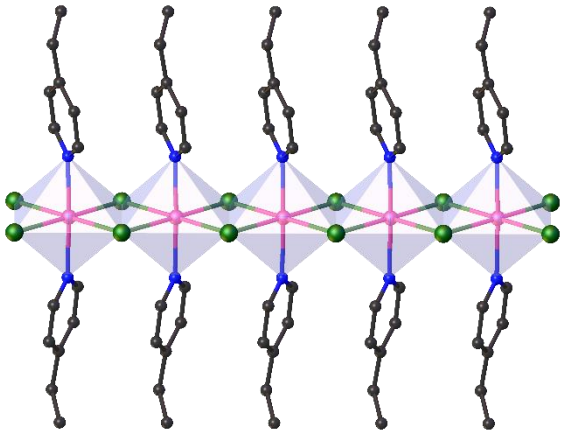


Figure 4. View of a single chain in $\{MnCl_2(4EtP)_2\}_n$.

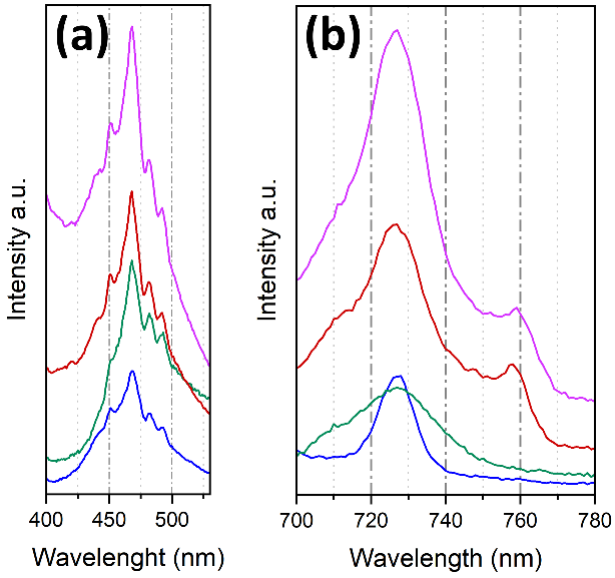


Figure 5. Solid-state PL spectra of $[MnCl_2(3AP)_4]$ (blue), $[MnBr_2(3AP)_4]$ (green), $\{MnCl_2(4EtP)_2\}_n$ (red), and $\{MnBr_2(4EtP)_2\}_n$ (magenta) in (**a**) the visible and (**b**) NIR regions. Data are split into two plots to avoid showing the excitation wavelength diffraction; the full PL spectra can be seen in Figure S12.

3. Conclusions

Different functional groups on pyridine ligands can be used to construct manganese halide materials with different dimensionalities. In the solid state, 0D or 1D materials with similar PL values were obtained, with key differences in the NIR emission peaks. Hydrogen bonding and changing the ligand ratio, cation, and metal ion are important factors that affect the dimensionality of the materials created. Under similar conditions, the halide atoms, chlorine, or bromine resulted in isomorphic structures, which were primarily supported by weak hydrogen bonds. Further studies will allow us to identify the main factors that affect the solid-state near-IR PL values of these types of materials.

4. Methods and Materials

All samples were phase pure, as shown by the powder X-ray diffraction (PXRD; Figures S5–S8). PXRD was performed using a Rigaku Ultima IV with Cu Kα radiation. Solid-state PL was collected using an RF-5301 PC Spectrofluorometer from Shimadzu. The solid was loaded in a special holder covered by a quartz slide and $[MnCl_2(3AP)_4]$ was analyzed with an excitation wavelength of 300 nm, $[MnBr_2(3AP)_4]$ and $\{MnCl_2(4EtP)_2\}_n$

with 340 nm, and finally **{$MnCl_2(4EtP)_2$}$_n$** with 350 nm. A thermogravimetric analysis was performed on an STA7200 from Hitachi. IR spectra were collected using Spectrum Two from PerkinElmer. Raman spectra were collected from solid samples using a DXR3 Smart Raman from Thermo Scientific. Solvents were obtained from commercial sources and used without further purification. The following reagents were purchased from commercial sources and used without further purification: manganese(II) chloride tetrahydrate (99%, Apolo Scientific, Chesire, UK), manganese(II) bromide tetrahydride (98%, Thermo Scientific, Ward Hill, USA), 4-ethylpyridine (98%, Sigma-Aldrich, St. Louis, USA), and 3-aminopyridine (99%, TCI America, Portland, USA).

[$MnCl_2(3AP)_4$]. In a 125 mL Erlenmeyer flask, $MnCl_2{\cdot}4H_2O$ (5.1 mmol, 1.01 g) was dissolved in 15 mL of ethanol using gentle heating, and then allowed to cool to room temperature. In a separate flask, 3-aminopyridine (20.4 mmol, 1.9 g) was also dissolved in 15 mL of ethanol using a gentle heating, and then allowed to cool to room temperature. Then, the 3-aminopyridine solution was added dropwise into the flask containing the solution of $MnCl_2$. Finally, the solution mixture was capped and left to crystalize for four days, resulting in light-brown crystals that were filtered and rinsed with cold isopropanol. The yield of dry product after filtration was 77%. IR ν (cm^{-1}): 3461(m), 3372(m), 3319(s), 3216(m), 3086(w), 3057(w), 3018(w), 2978(w), 2963(w), 1623(m), 1582(s), 1488(m), 1439(s), 1302(m), 1262(m), 1195(m), 1130(m), 1089(m), 1047(m), 1019(m), 968(w), 912(w), 898(w), 877(w), 849(m), 799(s), 700(s), 639(s), 543(m), 520(m), 487(w), 419(w), and 410(m).

[$MnBr_2(3AP)_4$]. In a 125 mL Erlenmeyer flask, $MnBr_2{\cdot}4H_2O$ (7.3 mmol, 1.6 g) was dissolved in 15 mL of ethanol using gentle heating, and then allowed to cool to room temperature. In a separate flask, 3-aminopyridine (29 mmol, 2.7 g) was also dissolved in 15 mL of ethanol using gentle heating, and then allowed to cool to room temperature. Then, the 3-aminopyridine solution was added dropwise into the flask containing the solution of $MnBr_2$. Finally, the solution mixture was capped and left to crystalize for four days, resulting in brown crystals that were filtered and rinsed with cold acetone. The yield of dry product after filtration was 44%. IR ν (cm^{-1}): 3454(w), 3414(w), 3370(w), 3316(s), 3215(m), 3086(w), 3054(w), 2977(w), 2963(w), 1622(m), 1591(w), 1581(s), 1487(s), 1442(s), 1351(w), 1302(m), 1281(w), 1263(m), 1198(m), 1139(m), 1089(m), 1049(m), 1020(m), 968(w), 943(w), 907(m), 878(w), 852(m), 829(w), 798(s), 700(s), 639(s), 543(m), 515(m), and 411(m).

{$MnCl_2(4EtP)_2$}$_n$. In a 125 mL Erlenmeyer flask, $MnCl_2{\cdot}4H_2O$ (5.1 mmol, 1.01 g) was dissolved with NaCl (2.6 mmol, 0.15 g) in 20 mL of isopropanol using gentle heating, and then allowed to cool to room temperature. Then, 4-ethylpyradine (10.2 mmol, 1.09 g) was added dropwise via a syringe into the flask containing the solution of $MnCl_2$. Finally, the solution mixture was capped and left to crystalize for a week, resulting in white crystals that were filtered and rinsed with cold isopropanol. The yield of dry product after filtration was 89%. IR ν (cm^{-1}): 3377(br), 3127(w), 3087(w), 3066(w), 3040(m), 3013(w), 2976(m), 2945(m), 2918(w), 2883(w), 1693(w), 1615(s), 1558(m), 1505(m), 1464(w), 1450(m), 1436(w), 1425(s), 1379(w), 1362(m), 1317(m), 1270(w), 1258(w), 1226(s), 12,059(w), 1108(w), 1079(s), 10,449(w), 1016(s), 994(w), 973(w), 869(m), 822(s), 780(s), 771(w), 721(m), 670(w), 600(w), 562(s), 487(s), and 422(w). Raman ν (cm^{-1}): 78(s), 118(s), 197(m), 239(w), 287(w), 400(w), 492(m), 566(w), 668(m), 784(m), 874(m), 1018(s), 1042(w), 1075(m), 1208(m), 1238(m), 1261(m), 1320(w), 1361(w), 1388(w), 1443(w), 1453(w), 1464(w), 1502(w), 1558(w), 1617(m), 2920(m), 2947(m), 2985(m), and 3070(s).

{$MnBr_2(4EtP)_2$}$_n$. In a 125 mL Erlenmeyer flask, $MnBr_2{\cdot}4H_2O$ (5 mmol, 1.06 g) was dissolved with NaBr (1.5 mmol, 0.15 g) in 20 mL of isopropanol by heating and allowed to cool to room temperature. Then, 4-ethylpyradine (10 mmol, 1.06 g) was added dropwise via a syringe into the flask containing the solution of $MnBr_2$. Finally, the solution mixture was capped and left to crystalize for 5 days, resulting in white crystals that were filtered and rinsed with cold acetone. The yield of dry product after filtration was 57%. IR ν (cm^{-1}): 3432(br), 3128(w), 3104(w), 3086(w), 3065(w), 3038(m), 3012(w), 2975(s), 2938(m), 2914(w), 2876(m), 1696(w), 1614(s), 1556(m), 1504(m), 1448(w), 1425(s), 1374(w), 1361(m), 1315(m), 1266(w), 1227(s), 1156(w), 1117(w), 1074(s), 1045(w), 1015(s), 992(w), 973(w), 953(w), 862(w),

823(s), 782(s), 715(m), 672(w), 639(w), 596(w), 560(m), 485(s), 426(w), and 404(w). Raman ν (cm^{-1}): 78(s), 406(w), 489(w), 562(w), 668(m), 784(m), 979(w), 1017(s), 1044(w), 1072(w), 1202(w), 1237(w), 1262(w), 1361(w), 1436(w), 1503(w), 1557(w), 1618(m), 2908(m), 2941(m), and 3069(s).

$[MnCl_3 3AP]^-[3APH]^+$. A sample of 3-aminopyridine (3AP) (20.3 mmol, 1882.2 mg) was dissolved in ethanol and slowly added into a flask containing a solution of $MnCl_2 \cdot 4H_2O$ (20.3 mmol, 4017.4 mg) and 13M HCl (1.6 mL) in ethanol. The molar ratio of 4AP to HCl to $MnCl_2 \cdot 4H_2O$ was 1:1:1, respectively. The solution mixture was dried in vacuo resulting in a pink solid that was then crystallized in methanol (using a slow evaporation technique) to obtain pale-pink crystals. After two weeks, the crystals were filtered out. The yield of dry product after filtration was 27%. IR ν (cm^{-1}): 3322(m), 3216(w), 3095(w), 2974(w), 1649(w), 1585(w), 1528(w), 1405(w), 1196(w), 997(w), and 760(w). Raman ν (cm^{-1}): 3098(m), 1659(w), 1532(w), 1238(w), 1047(m), 1000(s), 849(s), 826(w), 645(w), 528(w), and 410(w).

Supplementary Materials: The following supporting information can be downloaded at: https://www.mdpi.com/article/10.3390/cryst13121634/s1. Figures S1–S3: IR and Raman; Figure S4: View of a single layer of the coordination polymer within **$[MnCl_3 3AP]^-[3APH]^+$**; Figures S5–S8: Powder X-ray Diffraction Analysis; Figures S9–S12: TGA-DTA; Figure S13: Solid-state PL.

Author Contributions: Synthesis of all materials, A.P., K.G. and M.O.O.; IR and Raman characterization, A.P.; TGA and DTA analysis, A.P.; Photoluminescence, A.P. and M.O.O.; Single Crystal Data Collection, R.C.; figure preparation, A.P. and R.C.; original draft preparation, A.P. and R.C.; review and editing, R.C.; supervision, R.C.; funding acquisition, R.C. All authors have read and agreed to the published version of the manuscript.

Funding: This research was funded by NSF DMR PREM, grant number #2122108, and NSF DMR DMREF, grant number #2323548. The research reported in this publication was also supported by an Institutional Development Award (IDeA) from the National Institute of General Medical Sciences of the National Institutes of Health under grant number P20GM103451.

Data Availability Statement: The crystallographic data presented in this study are openly available on the CCDC database with the deposition numbers 2291444–2291448.

Conflicts of Interest: The authors declare no conflict of interest.

References

1. Roy, P.; Ghosh, A.; Barclay, F.; Khare, A.; Cuce, E. Perovskite Solar Cells: A Review of the Recent Advances. *Coatings* **2022**, *12*, 1089. [CrossRef]
2. Lekesi, L.P.; Koao, L.F.; Motloung, S.V.; Motaung, T.E.; Malevu, T. Developments on Perovskite Solar Cells (PSCs): A Critical Review. *Appl. Sci.* **2022**, *12*, 672. [CrossRef]
3. Pu, Y.; Su, H.; Liu, C.; Guo, M.; Liu, L.; Fu, H. A Review on Buried Interface of Perovskite Solar Cells. *Energies* **2023**, *16*, 5015. [CrossRef]
4. Lye, Y.-E.; Chan, K.-Y.; Ng, Z.-N. A Review on the Progress, Challenges, and Performances of Tin-Based Perovskite Solar Cells. *Nanomaterials* **2023**, *13*, 585. [CrossRef] [PubMed]
5. Abiram, G.; Thanihaichelvan, M.; Ravirajan, P.; Velauthapillai, D. Review on Perovskite Semiconductor Field-Effect Transistors and Their Applications. *Nanomaterials* **2022**, *12*, 2396. [CrossRef] [PubMed]
6. Paulus, F.; Tyznik, C.; Jurchescu, O.D.; Vaynzof, Y. Switched-On: Progress, Challenges, and Opportunities in Metal Halide Perovskite Transistors. *Adv. Funct. Mater.* **2021**, *31*, 2101029. [CrossRef]
7. Liu, X.-K.; Xu, W.; Bai, S.; Jin, Y.; Wang, J.; Friend, R.H.; Gao, F. Metal halide perovskites for light-emitting diodes. *Nat. Mater* **2021**, *20*, 10–21. [CrossRef]
8. Gao, P.; Cheng, S.; Liu, J.; Li, J.; Guo, Y.; Deng, Z.; Qin, T.; Wang, A. Facile Synthesis of Highly Emissive All-Inorganic Manganese Bromide Compounds with Perovskite-Related Structures for White LEDs. *Molecules* **2022**, *27*, 8259. [CrossRef]
9. Thien, G.S.H.; Ab Rahman, M.; Yap, B.K.; Tan, N.M.L.; He, Z.; Low, P.-L.; Devaraj, N.K.; Ahmad Osman, A.F.; Sin, Y.-K.; Chan, K.-Y. Recent Advances in Halide Perovskite Resistive Switching Memory Devices: A Transformation from Lead-Based to Lead-Free Perovskites. *ACS Omega* **2022**, *7*, 39472–39481. [CrossRef]
10. Thien, G.S.; Chan, K.-Y.; Marlinda, A.R. The Role of Polymers in Halide Perovskite Resistive Switching Devices. *Polymers* **2023**, *15*, 1067. [CrossRef]
11. Zhou, X.; Wang, Y.; Ge, C.; Tang, B.; Lin, H.; Zhang, X.; Huang, Y.; Zhu, Q.; Hu, H. Lead-Free Perovskite Single Crystals: A Brief Review. *Crystals* **2021**, *11*, 1329. [CrossRef]

12. Umar, A.; Sadanand Singh, P.K.; Dwivedi, D.K.; Algadi, H.; Ibrahim, A.A.; Alhammai, M.A.M.; Baskoutas, S. High Power-Conversion Efficiency of Lead-Free Perovskite Solar Cells: A Theoretical Investigation. *Micromachines* **2022**, *13*, 2201. [CrossRef] [PubMed]
13. Cieslik, P.; Comba, P.; Dittmar, B.; Ndiaye, D.; Tóth, É.; Velmurugan, G.; Wadepohl, H. Exceptional Manganese(II) Stability and Manganese(II)/Zinc(II) Selectivity with Rigid Polydentate Ligands. *Angew. Chem. Int. Ed.* **2022**, *61*, e202115580. [CrossRef] [PubMed]
14. Dube, K.S.; Harrop, T.C. Structure and properties of an eight-coordinate Mn(ii) complex that demonstrates a high water relaxivity. *Dalton Trans.* **2011**, *40*, 7496–7498. [CrossRef] [PubMed]
15. Baldeau, S.M.; Slinn, C.H.; Krebs, B.; Rompel, A. Five manganese(II) complexes with seven- or eight-coordinated Mn(II), revealing different coordination modes for the nitrato ligands. *Inorg. Chim. Acta* **2004**, *357*, 3295–3303. [CrossRef]
16. Morad, V.; Cherniukh, I.; Pöttschacher, L.; Shynkarenko, Y.; Yakunin, S.; Kovalenko, M.V. Manganese(II) in Tetrahedral Halide Environment: Factors Governing Bright Green Luminescence. *Chem. Mater* **2019**, *31*, 10161–10169. [CrossRef] [PubMed]
17. Xu, L.-J.; Sun, C.-Z.; Xiao, H.; Wu, Y.; Chen, Z.-N. Green-Light-Emitting Diodes based on Tetrabromide Manganese(II) Complex through Solution Process. *Adv. Mater.* **2017**, *29*, 1605739. [CrossRef]
18. Sen, A.; Swain, D.; Guru Row, T.N.; Sundaresan, A. Unprecedented 30 K hysteresis across switchable dielectric and magnetic properties in a bright luminescent organic–inorganic halide (CH6N3)2MnCl4. *J. Mater. Chem. C* **2019**, *7*, 4838–4845. [CrossRef]
19. Vinogradova, K.A.; Shekhovtsov, N.A.; Berezin, A.S.; Sukhikh, T.S.; Krivopalov, V.P.; Nikolaenkova, E.B.; Plokhikh, I.V.; Bushuev, M.B. A near-infra-red emitting manganese(II) complex with a pyrimidine-based ligand. *Inorg. Chem. Commun.* **2019**, *100*, 11–15. [CrossRef]
20. Stefańska, D. Effect of Organic Cation on Optical Properties of [A]Mn(H2POO)3 Hybrid Perovskites. *Molecules* **2022**, *27*, 8953. [CrossRef]
21. Long, G.J.; Clarke, P.J. Crystal and molecular structures of trans-tetrakis(pyridine)dichloroiron(II), -nickel(II), and -cobalt(II) and trans-tetrakis(pyridine)dichloroiron(II) monohydrate. *Inorg. Chem.* **1978**, *17*, 1394–1401. [CrossRef]
22. Yang, Q.-Y.; Chen, K.-J.; Schoedel, A.; Wojtas, L.; Perry Iv, J.J.; Zaworotko, M.J. Network diversity through two-step crystal engineering of a decorated 6-connected primary molecular building block. *CrystEngComm* **2016**, *18*, 8578–8581. [CrossRef]
23. Heine, M.; Fink, L.; Schmidt, M.U. 3-Cyanopyridine as a bridging and terminal ligand in coordination polymers. *CrystEngComm* **2018**, *20*, 7556–7566. [CrossRef]
24. He, X.; Lu, C.-Z.; Yu, Y.-Q.; Chen, S.-M.; Wu, X.-Y.; Liu, J.-H. trans-Tetrakis(3-aminopyridine)dichlorocadmium(II). *Acta Crystallogr. Sect. E* **2004**, *60*, m1639–m1640. [CrossRef]
25. Csöregh, I.; Kenessey, G.; Wadsten, T.; Liptay, G.; Carson, B.R. Pyridine type complexes of transition-metal halides XI. Structural, thermal and spectroscopic studies of aminopyridine complexes of cobalt(II) halides. *Z. Für Krist. Cryst. Mater.* **2000**, *215*, 547–552. [CrossRef]
26. Cain, B.R.; Freeman, J.M.; Henshall, T. Characteristic vibrations of the NH2 group. *Can. J. Chem.* **1969**, *47*, 2947. [CrossRef]
27. Su, C.-W.; Wu, C.-P.; Chen, J.-D.; Liou, L.-S.; Wang, J.-C. Synthesis and structural characterization of two chain complexes of Mn(II) containing 2-aminopyridinium. *Inorg. Chem. Commun.* **2002**, *5*, 215–219. [CrossRef]
28. Brede, F.A.; Mühlbach, F.; Sextl, G.; Müller-Buschbaum, K. Mechanochemical and thermal formation of 1H-benzotriazole coordination polymers and complexes of 3d-transition metals with intriguing dielectric properties. *Dalton Trans.* **2016**, *45*, 10609–10619. [CrossRef]
29. Lee, L.M.; Elder, P.J.W.; Dube, P.A.; Greedan, J.E.; Jenkins, H.A.; Britten, J.F.; Vargas-Baca, I. The size of the metal ion controls the structures of the coordination polymers of benzo-2,1,3-selenadiazole. *CrystEngComm* **2013**, *15*, 7434–7437. [CrossRef]

Disclaimer/Publisher's Note: The statements, opinions and data contained in all publications are solely those of the individual author(s) and contributor(s) and not of MDPI and/or the editor(s). MDPI and/or the editor(s) disclaim responsibility for any injury to people or property resulting from any ideas, methods, instructions or products referred to in the content.